Tip-Vortex Localization for Cross-Stream Position Control of a Multi-Hole Probe Relative to a Stationary Wing in a Free-Jet Wind Tunnel

Nathan Lauer,[1] Derrick Yeo,[2] David Snyder,[3] and Derek A. Paley,[4]
Collective Dynamics and Control Laboratory
University of Maryland, College Park, MD, 20740

The continuing development of fully autonomous aircraft requires advanced sensing and control systems in order to complete difficult tasks such as aerial refueling and close formation flight. To accomplish such maneuvers, an aircraft must be able to measure the location of nearby aircraft and position itself relative to these other flight vehicles. In visually degraded environments where vision sensors might struggle, wake sensing provides an effective means of locating other aircraft. Using onboard velocity measurements, we combine a point-vortex model with a Bayesian filter to estimate a leader aircraft location through the sensing of wingtip wake vortices. We demonstrate the filtering strategy by estimating the position of a wing using experimental data in an open-jet wind tunnel. An experimental test-bed rapidly positions a flow measurement system within the wake of a wing in a free stream. A flow survey of the tip vortex within the aerodynamic wake of a leader aircraft, conducted with a multi-hole probe, measures velocities in the cross-stream plane. The wake position estimates are used for closed-loop control of the sensor position. This paper presents the estimation strategy and model, experimental data, closed-loop control simulation, and real-time wind tunnel feedback control results. In ongoing work, we are considering applications in which a follower aircraft senses the wake of a leader aircraft and positions itself for maximum aerodynamic efficiency.

Nomenclature

C_{D_i}	=	induced drag coefficient for leader aircraft wing
C_L	=	coefficient of lift for leader aircraft wing
D_i	=	induced drag on leader aircraft wing
V_∞	=	flow velocity ahead of aircraft.
V_i	=	velocity vector component in i^{th} direction
$\boldsymbol{b}_i$	=	i^{th} unit vector of frame B
$\vec{\boldsymbol{r}}$	=	position vector of follower aircraft relative to leader aircraft
$\boldsymbol{x}_k$	=	observed measurement at step k
$\boldsymbol{z}_k$	=	state at step k
ρ_∞	=	density of flow ahead of aircraft
B	=	body reference frame of follower aircraft
L	=	lift force acting on a wing
O	=	origin of body reference frame for follower aircraft
P	=	proportional gain in closed-loop control

[1] Undergraduate Student, Aerospace Engineering and Computer Science, 3711 Campus Dr. College Park, MD, 20740, AIAA Student Member.
[2]Assistant Research Scientist, Aerospace Engineering Department, 8320 Baltimore Ave., College Park, MD, 20742
[2]Assistant Research Scientist, Aerospace Engineering Department, 8320 Baltimore Ave., College Park, MD, 20742 dyeo@umd.edu, AIAA Member.
[3]Undergraduate Student, Aerospace Engineering, 7524 Calvert Service Ln. College Park, MD, 20740, AIAA Student Member.
[4]Willis H. Young Jr. Associate Professor of Aerospace Engineering Education, Department of Aerospace Engineering and Institute for Systems Research, 3150 Martin Hall, College Park, MD, 20742, AIAA Associate Fellow.

S = wing area of leader aircraft
b = wingspan of leader aircraft
r = radial distance from vortex center
Γ = vortex circulation strength
φ = flow potential function used to describe wake

I. Introduction

The National Airspace System is growing increasingly crowded, and research is being conducted to allow aircraft to fly closer together. While the ongoing work in the Air Traffic Control's Next Generation system is undoubtedly improving flight paths for a higher volume of aircraft, there is also much to be gained by developing systems enabling safe and coordinated formation flight. Close-formation flight allows for an extended range with aerial refueling,[1,2] increases in fuel efficiency,[3,4] and an organization method for commercial aircraft flight procedures.[5] To safely achieve these benefits, we need to develop automatic-control strategies for aerodynamic sensing and control of aircraft in close-formation flight.

In previous work by DeVries and Paley[6], observability-based control strategies were presented for aircraft in close-formation flight, in which a grid-based Bayesian filter was used for wake estimation and measures of observability to quantify regions of degraded performance. This paper develops these ideas further by testing them in a wind tunnel, utilizing a point vortex model for the wake of a leader aircraft and a grid-based Bayesian filter for wake estimation. Simulations with wind tunnel data demonstrate the feasibility of using wake estimation as a viable method for close-formation flight control. The wake estimation strategy is performed using feedback control in real time in an open-jet wind tunnel.

There is a large body of work modeling close-formation flight, not only in human-designed aircraft but also in bird formations.[7] Many of these papers use lifting-line theory or vortex lattices to estimate various wake parameters. Furthermore, many of the papers that extend the aerodynamic sensing to control simulations of aircraft in formation flight use extended Kalman filters or particle filters.[8,9] However, we implement the control algorithms in real time in a wind tunnel, assuming known kinematics of the leader aircraft, using a grid-based Bayesian filter. DeVries and Paley[6] introduced the idea of using a grid-based Bayesian filter for wake estimation, and we demonstrate the viability of this idea in an experimental setting.

The main contributions of this paper are as follows: (1) a novel experimental test-bed for real-time differential-pressure airspeed sensing in a wind tunnel; (2) a demonstration of the feasibility of using a grid-based Bayesian filter to do wake estimation in a formation-flight control algorithm; and (3) real-time feedback control for localization of a multi-hole probe in an active wind tunnel relative to a stationary wing. This work demonstrates a technique that uses real-time flow measurements for advantageous positioning within a flow field.

The organization of this paper is as follows: Section II describes the aerodynamic model used to represent to aircraft in formation flight and the Bayesian filter used for wake estimation. Section III describes the experimental design and setup in the wind tunnel. Section IV presents the results from the wind tunnel tests, simulations run from that data, and the results of using the wake-estimation strategy with feedback control in an active wind tunnel. Section V presents conclusions and ongoing work.

II. Leader Aircraft Aerodynamic Sensing

This section describes the aerodynamic modeling of two aircraft flying in close formation, where the wake from the leader aircraft affects the aerodynamics of follower aircraft. In particular, Section II.A describes the reference frames of the two-aircraft formation and the vortex model used to model the wake of the leader aircraft. Section II.B reviews recursive Bayesian filtering, which is used to estimate the position of the wingtip vortex of the leader aircraft.

A. Two-Aircraft Aerodynamic Model

This section develops an aerodynamic model to describe two aircraft flying close together. One aircraft acts as the leader; the other is a follower. For the purpose of this work, assume that the two aircraft are flying in steady, level flight through an inviscid, irrotational, and incompressible fluid. Consider the

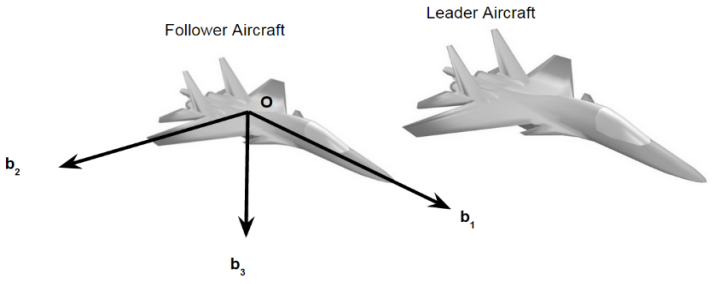

Figure 1. *Body reference frame B on the second aircraft in close formation flight.*

follower's body reference frame $B = (O, \boldsymbol{b_1}, \boldsymbol{b_2}, \boldsymbol{b_3})$, with O centered along the longitudinal, lateral, and vertical axes of the follower aircraft. Reference frame B is shown in Figure 1. Note that $\boldsymbol{b}_3$ is positive downwards and $\boldsymbol{b}_1$ is positive towards the leader aircraft. The leader has wingspan b, and is positioned relative to the follower aircraft by $\vec{\boldsymbol{r}} = x\boldsymbol{b}_1 + y\boldsymbol{b}_2 + z\boldsymbol{b}_3$. We assume that the leader aircraft maintains steady flight without any rapid or drastic changes, and that the follower aircraft maintains kinematic control of the longitudinal distance x between the two aircraft. In this case, the transverse velocity of the follower aircraft relative to the leader aircraft is

$$V_{follower} = V_y\boldsymbol{b}_2 + V_z\boldsymbol{b}_3 \tag{1}$$

In order to implement a controller allowing the follower aircraft to position itself strategically relative to the leader aircraft, we use a model of the aerodynamic wake of the leader aircraft. Since the flow is irrotational, we apply potential flow theory. In fluid dynamics, a potential flow is a representation of the velocity field of a fluid[10] obtained by taking the gradient of the velocity potential φ, which is a scalar potential function of space and time. (In a scalar potential, the difference in potential energy of two particles in the flow depends only on the position of the particles, and not on the particle paths.[11])

Thus, the velocity field is the rate of change of the potential energy of all particles in the flow, where the potential energy of each particle is independent of its time history. The velocity field satisfies[11]

$$V = \nabla\varphi. \tag{2}$$

Since the curl of the gradient of the function[10] is

$$\nabla \times V = 0\,, \tag{3}$$

the vorticity of the flow is zero and, therefore, a potential flow is irrotational.[10] Further, since our flow is incompressible, the velocity field has zero divergence, which implies that the velocity potential must satisfy Laplace's equation[10]

$$\nabla^2\varphi = 0. \tag{4}$$

Therefore, because potential flow theory is applicable in this flow, we are not concerned with the flow inside a boundary layer, and since the follower aircraft is at least two wingspans behind the leader aircraft,[12] the wake of the leader aircraft may be approximated as the sum of two infinite line vortices, each with circulation strength Γ. The existence of these vortices can be explained by the Kutta-Joukowsky theorem, which describes the lift on an airfoil due to circulation in the flow caused by the pressure differential above and below the airfoil[13] as

$$L = \rho_\infty V_\infty \Gamma\,. \tag{5}$$

This circulation implies that there exist wingtip vortices, and the induced velocity of one of these vortices is described[14] by

$$V_\theta = \frac{C_L V_\infty}{5.341 A \bar{r}}, \tag{6}$$

where $A = b^2/S$ is the wing aspect ratio and $\bar{r} = 2r/b$. More simply

$$V_\theta = \frac{C}{r}, \tag{7}$$

where the total circulation C is constant. Eq. (7) is the equation for a point vortex. Thus, in this work the wake of the leader aircraft is sufficiently described by a point-vortex model. (Although we considered more complex vortex models, such as a Rankine vortex, these models did not perform as well experimentally as the point vortex model – likely due to measurement noise.)

Finally, we do not consider movement on the part of the leader aircraft. Assume that the vortex generation is a constant process, yielding a vortex that itself is constant in space and time for the implementation of the Bayesian filter.

B. Bayesian Filtering and Estimation

In order to estimate the relative location of the leader aircraft, the follower aircraft measures the wake of the leader aircraft using differential-pressure measurements. These measurements are used as input to a grid-based recursive Bayesian filter, which outputs a probability density of the location of the center of the leader's wingtip vortex. The cross-stream space behind the leader aircraft is divided into a uniform grid and, after the follower aircraft measures the incoming airflow, each grid point is assigned the probability of the wingtip vortex center existing at that grid-point location. Recursive Bayesian estimation is the process of generating this probability density function and letting it evolve through time.

In general, a Bayesian filter consists of a prediction step and an update step to estimate an unknown probability density function over the states of the system. Each state is assumed to be an unobserved Markov process; the current true state at time t_i depends only on the previous state at time t_{i-1}. Each successive step uses the previous probability density function as a prior distribution, generates a new probability density function over the same state space based on the incoming measurements, and then multiplies the two densities together to obtain a posterior distribution. Often, the filter starts from a uniform distribution; when measurements of the states are taken the update step is run and information is gained about the system. At time steps when no new measurements have been taken, only the prediction step is run, and information about the system diffuses. New measurements of the state are incorporated using Bayes' theorem in the update[15] step:

$$P(\boldsymbol{x}_k|\boldsymbol{z}_k) = \frac{P(\boldsymbol{z}_k|\boldsymbol{x}_k)P(\boldsymbol{x}_k|\boldsymbol{z}_{1:k-1})}{P(\boldsymbol{z}_k)}. \tag{8}$$

When no new information has arrived, the probability density function is updated according[15] to

$$P(\boldsymbol{x}_k|\boldsymbol{z}_{1:k-1}) = \int P(\boldsymbol{x}_k|\boldsymbol{x}_{k-1})P(\boldsymbol{x}_{k-1}|\boldsymbol{z}_{1:k-1})d\boldsymbol{x}_{k-1}. \tag{9}$$

Thus, a Bayesian filter maintains an estimate of the state of the system by assimilating new data as it arrives, and evolving the estimate at time steps when no new information is available.

There are three general types of Bayesian filters: the Kalman filter, the particle filter, and grid-based estimators.[16] A grid-based filter is used here because of the nonlinear measurement model and because we only estimate two states. In this work, the state of the system X is the center of the lead wingtip, represented by two terms (the vortex strength is assumed known):

$$\boldsymbol{X} = \begin{bmatrix} Y \\ Z \end{bmatrix}. \tag{10}$$

Let V_y, V_z be the cross-stream velocities of the vortex flow field. The follower aircraft takes airflow measurements at different locations in the grid-space to obtain V_y and V_z. That information is used as the first term in Bayes' theorem in the update step of the filter.

Assuming that the measurement noise is normally distributed, the likelihood function is

$$P(\boldsymbol{z}_k|\boldsymbol{x}_k) = exp\left[-\frac{\left(V_y - \tilde{V}_y\right)^2 + \left(V_z - \tilde{V}_z\right)^2}{\sigma^2}\right] \tag{11}$$

where σ is the uncertainty in the sensor uncertainty, measurement noise, and $\tilde{V}_y$, $\tilde{V}_z$ are predicted by the point vortex model. Note that this likelihood function uses Cartesian coordinates and assumes equal measurement uncertainty in V_y and V_z. Using polar coordinates may be more effective, because we have empirically observed the radial and azimuthal noise densities to be different.

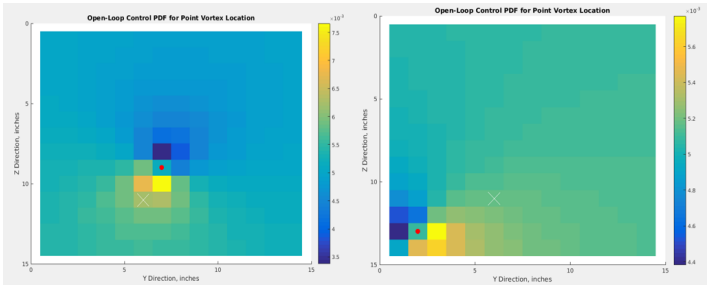

Figure 2. *Sample likelihood functions. The red dot is the sensor location, while X is the estimated vortex center from gathered data.*

The likelihood function is multiplied by the prior distribution – the second term in the numerator of Bayes' theorem – and the resulting posterior distribution is normalized. Figure 2 shows some example likelihood functions.

The estimation process runs in real time. Each measurement yields an improved estimate for the location of the wingtip vortex of the leader aircraft. The filtering and estimation technique is summarized in Figure 3. The next section describes open- and closed-loop control algorithms that position the follower aircraft strategically relative to the leader aircraft wingtip position.

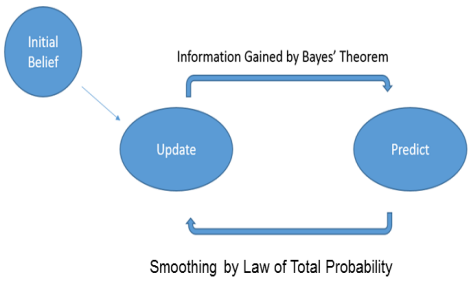

Figure 3. *Flow chart for a Bayesian filter.*

III. Experimental Design

We ran several wind tunnel experiments: a survey of the wind tunnel's flow field with no model in the critical section, a series of raster scans of the wake of the leader aircraft at various downstream distances, and several closed-loop localization tests. Further control simulations were run using that data, in addition to an offline closed-loop control experiment. The following section describes the setup used to run the wind tunnel tests and flow surveys.

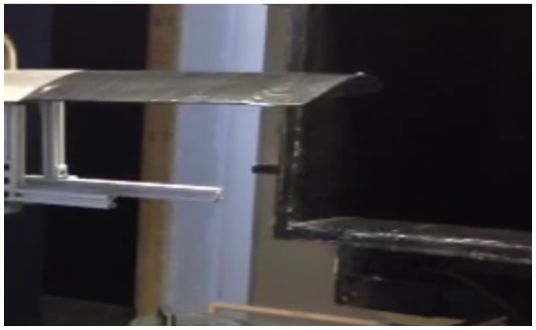

Figure 4. *The right wing of the leader aircraft mounted so that the wingtip is centered in the wind tunnel flow.*

A. Leader Aircraft and Multi-Hole Airspeed Probe

The leader aircraft in this work is represented by a single half-wing airfoil (the right-hand wing). Since we are modeling its wake as a wingtip vortex, a stronger vortex makes measurement and estimation easier. Wingtip vortices are a consequence of the induced[13] drag

$$D_i = \frac{1}{2}\rho V^2 S C_{D_i}, \tag{12}$$

where S is the area of the wing. Thus, the larger the wing, the stronger the vortex, and the easier it is to measure. The right wing is mounted just outside the wind tunnel's test section (see Section IV.B) with its tip extending to the middle of the test section. The wing chord is 8 inches with a 36-inch span, and is mounted as shown in Figure 4.

For the follower aircraft to accurately measure the wake of the leader aircraft, an airspeed probe would have to be placed in front of the follower aircraft, such that the airflow over the body of the follower aircraft does not interfere with the flow measurements. As such, for the purposes of this work, a physical wind-tunnel model of the follower aircraft is deemed unnecessary, and the follower aircraft is instead represented by only the pressure-based airspeed probe.

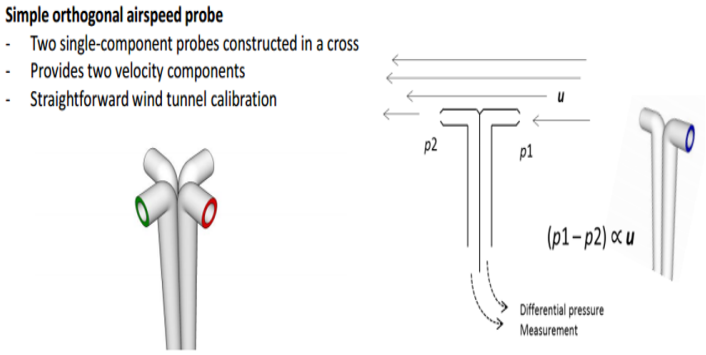

Figure 5. *The flow probe*[17] *used for bi-directional differential pressure measurements.*

The multi-hole probe consists of four metal tubes in pairs of two. In each pair, the tubes point in opposing directions, so that a differential pressure measurement is obtained at that location[17]. In total, the probe gives two orthogonal velocity measurements at its location. These probes (see Figure 5) are advantageous[17] due to improved noise characteristics and resolution at low speed, ease of fabrication, and simultaneous multi-direction sensing.

The probe is mounted in the University of Maryland Free-Jet Wind Tunnel on a large, heavy gantry that provides full three-dimensional motion. The gantry can be operated autonomously to follow specific patterns, or can be operated manually in real time to send the probe to any location. The gantry is positioned behind the leader aircraft wing according to the reference frame defined in Section II.A. To move the probe, a PWM signal is sent to two servo motors, which together move the probe to the desired location. The servo command conventions make it simpler for downwards to be defined as positive. Therefore, the reference frame is defined with $\boldsymbol{b}_3$ positive downwards, as shown in Figure 1. The combination of this gantry and airspeed probe is one of the primary contributions of this work; the probe can be moved in any direction or pattern in real-time while the wind tunnel is in operation, which allows us to step outside the bounds of traditional wind tunnel testing.

B. Wind Tunnel

The wind tunnel we use is has an open test section and the air is not recycled. In this sense, the test section is not isolated from influences outside the test area. Therefore, the wing mount and multi-hole airspeed probe must be placed so that the data is not affected by the interaction between the wind tunnel airflow and the standing atmospheric air. The wind tunnel has a maximum downstream flow velocity of $15\ m/s$. A mechanical anemometer was used to obtain a ground truth of the free-stream flow velocity, and for the linear calibration of the multi-hole probe.

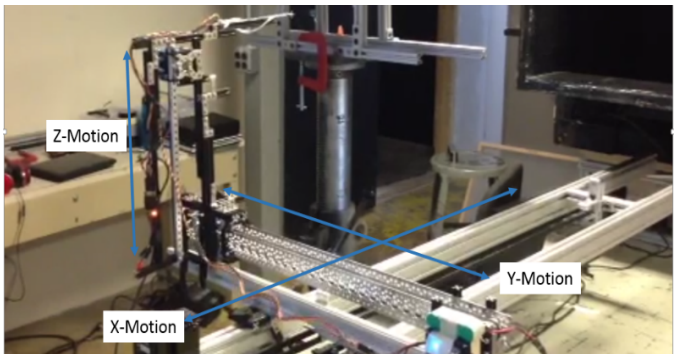

Figure 6. *The flow probe mounted on the Cartesian gantry, which allows motion in three directions.*

IV. Experimental Results

This section describes the results of the wind tunnel tests. The first experiments run in the wind tunnel were raster scans at various downstream locations, described in Section IV.A. Section IV.B and Section IV.C were performed as simulations outside of the wind tunnel, using the data taken during the raster scan; any time during the simulation the probe was instructed to take a reading, we look up the measurement in the raster scan data at the relevant location, and return that value as the measurement value. Section IV.D describes closed-loop control results from real-time experiments in the wind tunnel.

A. Flow Survey

We performed a flow survey in order to obtain a baseline for the wind tunnel's airflow without the leader wing. By establishing a baseline in which there is little to no cross-stream velocity, we verify that any significant cross-stream velocity measured in the raster-scans is due to the wake of the leader aircraft. Figure 7 shows the cross-stream velocities of the baseline survey. Each arrow represents a measurement taken at that location, the direction of the arrow indicates the direction of the flow, and the length of the arrow represents the relative magnitude. Note that since the arrow length is relative magnitude and not absolute magnitude, the velocities appear to be of the same magnitude as seen in the next section. However, this is not the case, as each measurement here is normalized by the maximum measurement taken, for easy visualization. The maximum value is less than one quarter of the maximum velocity seen in the next section.

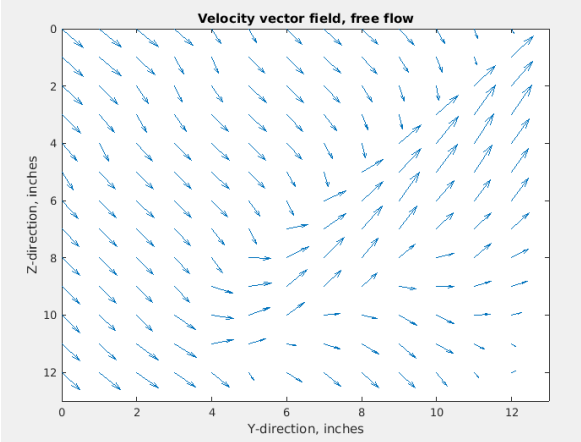

Figure 7. *Open test-section flow survey. Note that arrows are drawn larger than scale.*

B. Open-loop Flow Surveys

Next, we determined if there actually is a wingtip vortex present, or more accurately, a vortex that is strong enough to be sensed. The strength and size of the vortex is linearly dependent on the size of the wing and the amount of lift that the wing produces. Since we use a relatively small wing and relatively low flow velocity, it is possible that the wingtip vortex is not strong enough to sense. As a test, two visualization experiments were run. First, we

introduced smoke in front of the wing to visualize the airflow. As can be seen in Figure 8, a region of circular flow was observed around and behind the wingtip, suggesting that this flow condition was suitable for continued testing. We surveyed the flow behind the wing by taking a series of vertical and cross-stream velocity measurements at four downstream locations. In each scan, we divided the cross-stream plane into a 14x13 grid, and took velocity measurements at each grid point using a pressure-based airspeed probe[17]. From this data, quiver and vorticity plots were constructed at each of the various downstream locations. As seen in Figure 9, there does appear to be a wingtip vortex. Based on our measurements, we predict the vortex center to be at the location of highest vorticity. The plots in Figure 10 show the data taken at each downstream location. Figure 11 shows vorticity slices of the cross-stream flow behind the wing. The red sections indicate high positive (counterclockwise) vorticity, while blue indicates high negative (clockwise) vorticity. The plots are generated from data taken by the multi-hole probe during the raster scan wind tunnel test. From this plot, it is clear that the multi-hole probe and estimation technique are capable of sensing the wingtip vortex.

Figure 8. *Introducing smoke into the wind tunnel flow. The resultant spreading of the smoke indicates that there is some change in the flow across the airfoil.*

C. Open-Loop Control Results

An open-loop controller does not involve the use of feedback to make control decisions. In this case, the probe follows a pre-planned trajectory that is independent of the readings the flow probe takes. Open-loop control is useful for demonstrating the Bayesian estimation process in a step-by-step fashion, and as an initial indicator of closed-loop feasibility. In this subsection, the control was performed as a simulation outside of the wind tunnel. Therefore, anytime a measurement is taken in the simulation, we look up the value that the probe took at that location in the raster scan data. Each simulation uses real, experimental data.

A single step in the estimation and control loop is demonstrated in Figure 12, in which the control process has been paused at an intermediate time step. In this instance, the flow-probe is at location (8 inches, 8 inches), with a prior distribution as shown in the left image in Figure 12. This prior distribution was obtained at the previous time-step, and was the result of the estimation process and flow measuring as described in Section III.B. Next, the flow probe is commanded to take a new measurement, which generates a measurement likelihood function as in the center image in Figure 12. That likelihood function is multiplied by the prior distribution and normalized according

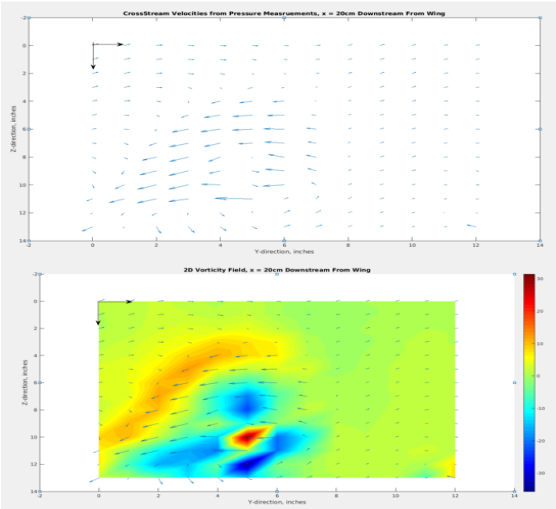

Figure 9. *Quiver plot of cross-stream flow velocity two wingspans downstream of the airfoil (top), with the resulting vorticity visualization (bottom).*

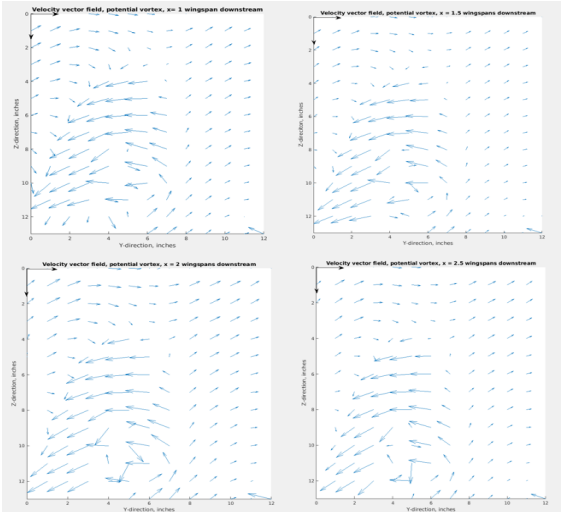

Figure 10. *Progressive slices of the cross-stream velocity field, at 1, 1.5, 2, and 2.5 wingspans downstream of the airfoil.*

to Bayes' theorem, which results in the new posterior distribution, the right-hand image in Figure 12. This posterior distribution is now a new probability density function representing the current best estimate for the location of the center of the vortex.

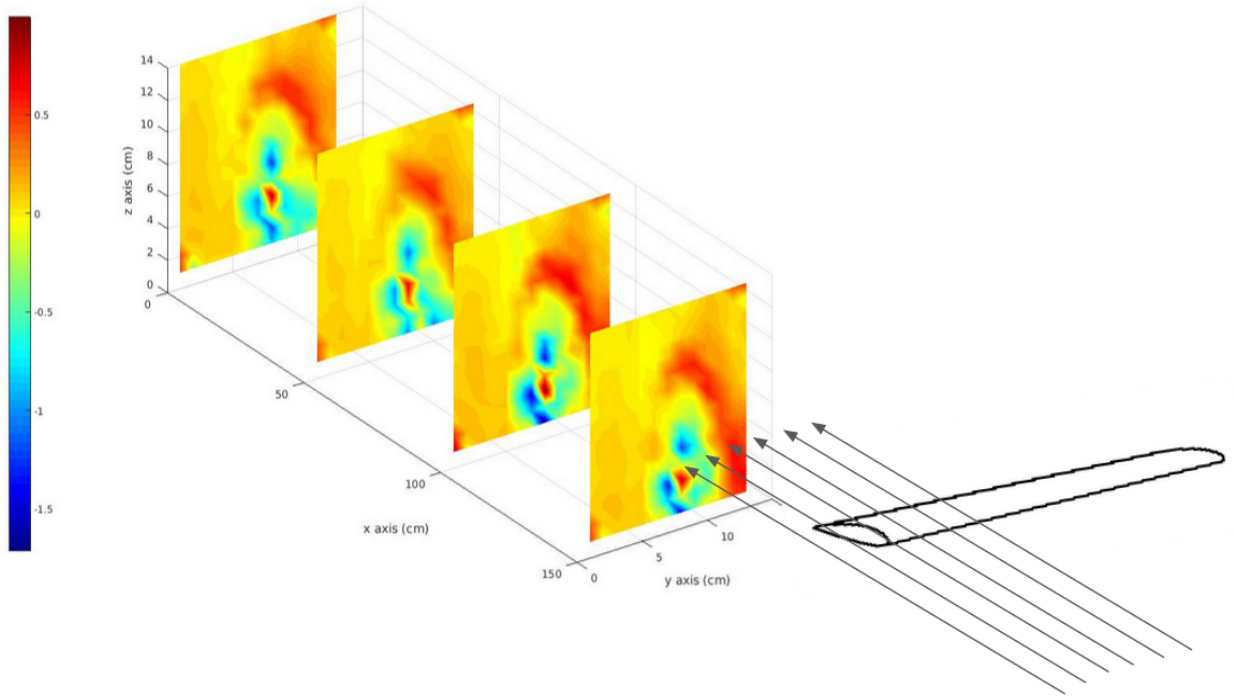

Figure 11. *Vorticity slices of the cross-stream flow behind the wing.*

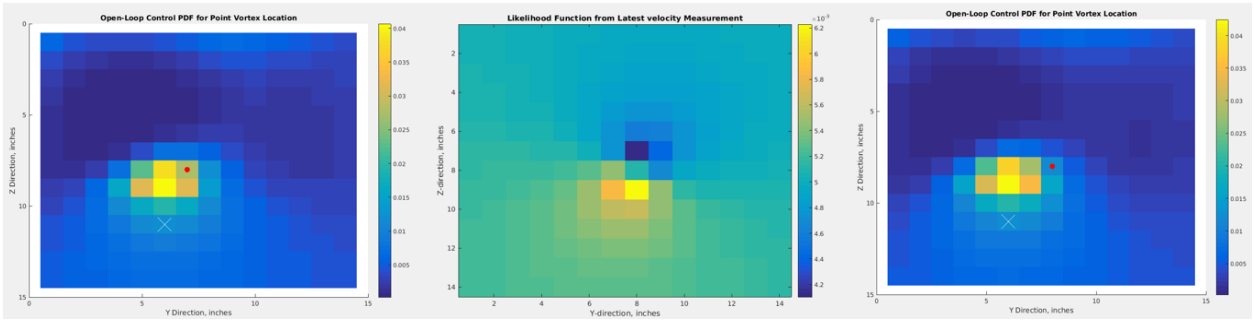

Figure 12. *A single step in open-loop control, illustrating the Bayesian filter process. The prior distribution (left) is multiplied by the airspeed measurement-generated likelihood function (center) to form the posterior distribution (right).*

In the case of a preplanned trajectory, the probe follows the same path as in the raster scan. As mentioned above, each measurement taken by the probe is obtained from a lookup table built from the raster scan data. Using the lookup table, we track the probability density function of vortex location as it evolves through time. Figure 13 shows how the probability density function changes as an increasing number of measurements are taken.

Initially, when the probe is far away from the vortex center, little information is obtained from a measurement taken, and so the probability density function is nearly uniform. At a later time, when more measurements have been taken, and the probe is closer to the vortex center, the probability density function makes a better prediction of the vortex center. Finally, once the probe is scanning near the area of the vortex center, each measurement reinforces the previous prediction, and the estimate grows stronger. This strengthening is observed in higher-resolution open-loop tests, as well as closed-loop simulation and real-time testing as described in the following section.

D. Closed-Loop Control Results

Next we describe closed-loop control experimental results. That is, the system used feedback control to send commands to the gantry in real time. The complete algorithm is described in Figure 14. We implemented a controller that uses observer-based feedback control. The controller uses a fixed-interval movement system; at each step it moves in 0.80-inch increments towards the expected mean. In simulations, the controller was proportional with a gain of 0.5. Figure 15 shows the progression of the controller in simulation. The background is the probability density function at each time-step, the red dot represents the current location of the sensor, and the yellow dot represents the computed next point to move. As can be seen, the gantry eventually converges to the estimated vortex center location.

Subsequent closed-loop control was successfully implemented in offline and real-time wind tunnel testing. However, because the estimator would not get reliable information from an estimate far away from the vortex (see Figure 10), four to nine initialization points were randomly chosen and readings were aggregated from these points before beginning the closed-loop localization cycle. The vortex center was verified using a cross-stream flow sensor and the measured wingtip position. Figure 16 shows two successful tests. The real-time test with accompanying velocity quiver shows a localization around a clear vortex center near (56, 56), or (7.28, 5.6) inches. The offline test, using prior raster scan data, shows the localization around a vortex near (44, 44), corresponding to (5.72, 4.4) inches, with the corresponding velocity quiver plot.

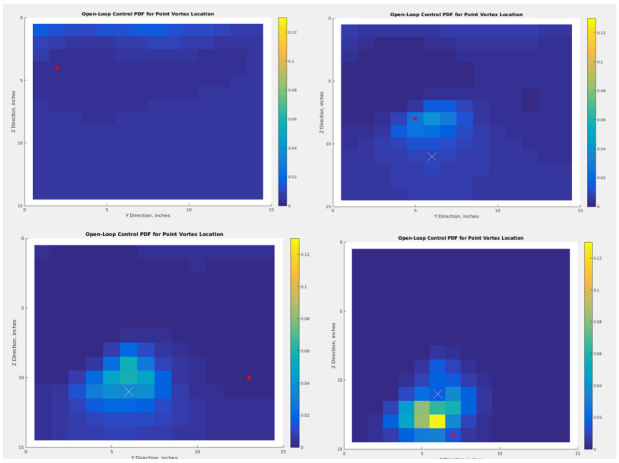

Figure 13. *Open-loop control for a pre-planned trajectory. From left to right, top to bottom, the probe moves closer to the estimated vortex center, and the distribution function updates as new data is assimilated.*

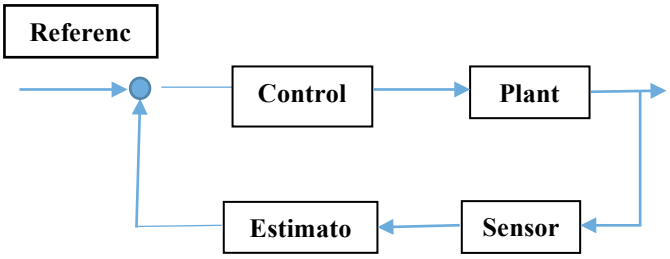

Figure 14. A *block diagram for a closed-loop control strategy. The 'Plant' moves the probe, the 'Sensor' measures the probe reading, the 'Estimator' is a Bayesian filter, and the 'Control' is a normalized proportional controller.*

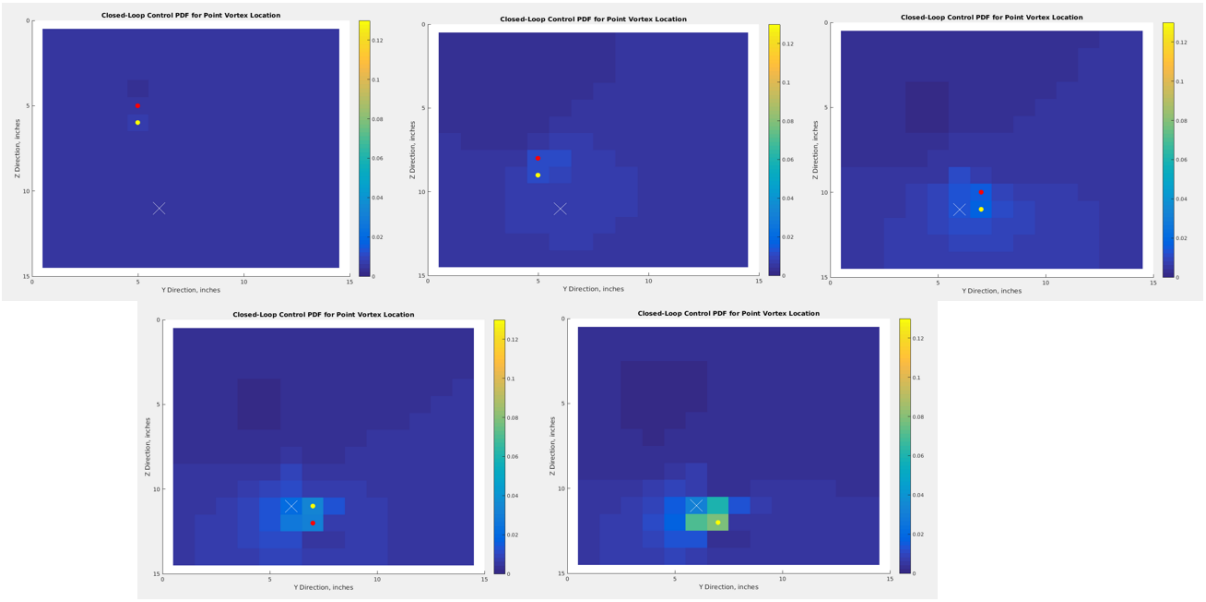

Figure 15: *A left to right, top to bottom, progression of snapshots from the closed-loop control simulation, marking the current probe location (red dot), the target location (yellow dot), and the estimated vortex center (white 'X').*

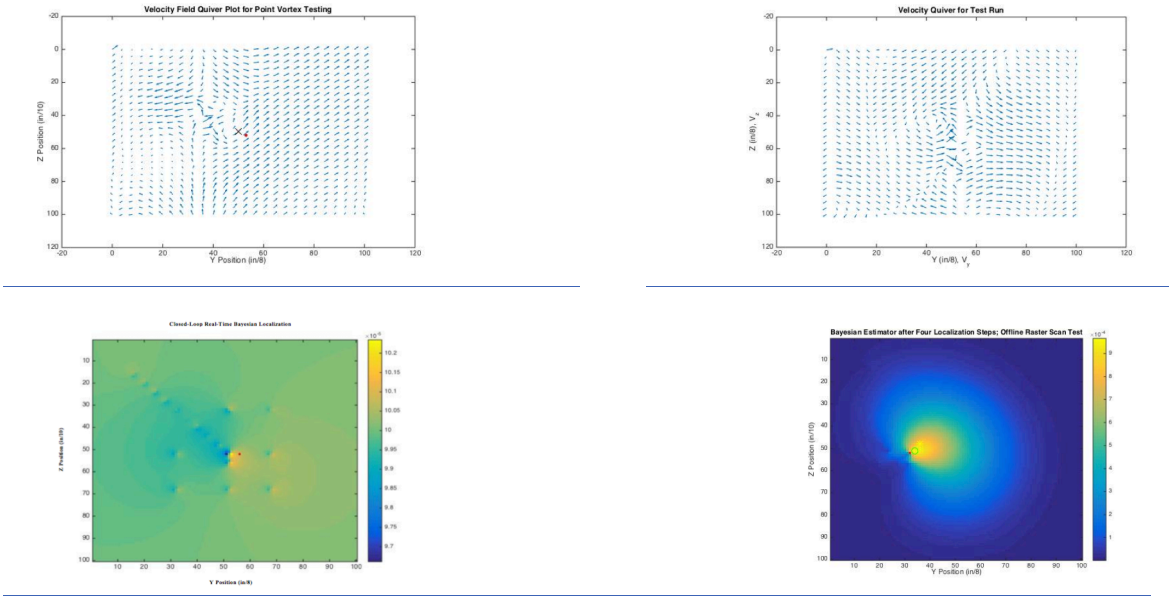

Figure 16. *(L) Real-time closed-loop test results with velocity field quiver plot (top) and final localization point (bottom). The red dot represents the estimated vortex center. (R) Offline testing using a different raster scan survey. The maximum corresponds to (5.72, 4.4) inches (top) and the control loop properly localizes after several more iterations.*

V. Conclusions

This paper describes a novel experimental test bed for formation-flight using flow estimation. We estimate location of the aerodynamic wake of a stationary wing in a wind tunnel, representing a leader aircraft in formation flight. To obtain this estimate, we measure data using onboard flow probes and filter the data through a Bayesian estimator to output a probability density function representing the position likelihood of the wing-tip vortex created by the wing. That data is then used in open- and closed-loop controllers to position the flow probe strategically relative to the leader wing.

The results indicate that the novel test-bed is capable of sensing the wingtip vortex, and that real-time control in an active wind tunnel is feasible. Furthermore, strongest closed-loop implementation occurs with a combination of closed-loop control and an open-loop selection of several random initialization points; this combination resulted in successful localizations in real-time testing.

Acknowledgements

The authors would like to thank Frank Lagor, Brian Free, and Elena Shrestha for discussions related to this work. They would also like to thank Dr. Allen Winkelmann for the use of the University of Maryland Free-Jet Wind Tunnel. Finally, the authors would like to thank Sarah-Leah Thompson for her assistance in creating several of the figures used in this paper.

References

[1]Dogan, A., Sato, S., and Blake, W., "Flight Control and Simulation for Aerial Refueling," *AIAA Guidance, Navigation, and Control Conference*, AIAA Paper 2005-6264, Aug. 2005.

[2]Dogan, A., Lewis, T. A., and Blake, W., "Flight Data Analysis and Simulation of Wind Effects During Aerial Refueling," *Journal of Aircraft*, Vol. 45, No. 6, 2008, pp. 2036–2048. doi:10.2514/1.36797

[3]Blake, W., and Multhopp, D., "Design, Performance, and Modeling Considerations for Close Formation Flight*," AIAA Guidance, Navigation, and Control Conference*, AIAA Paper 1998-4343, Aug. 1998.

[4]Maskew, B., "Formation Flying Benefits Based on Vortex Lattice Calculations," NASA CR-151974, 1974.

[5]Kent, T. E., and Richards, A. G., "A Geometric Approach to Optimal Routing for Commercial Formation Flight," *AIAA Guidance, Navigation, and Control Conference*, AIAA Paper 2012-4769, Aug. 2012, doi:10.2514/6.2012-4768

[6]DeVries, Levi, and Derek A. Paley. "Wake estimation and optimal control for autonomous aircraft in formation flight." *Proc. of AIAA Guidance, Navigation, and Control Conf., Boston, MA*. 2013.

[7]Hummel, D., "Aerodynamic Aspects of Formation Flight in Birds," *Journal of Theoretical Biology*, Vol. 104, No. 3, 1983, pp. 321–347. doi:10.1016/0022-5193(83)90110-8

[8]Katz, J., and Plotkin, A., Low-Speed Aerodynamics, 2nd ed., Cambridge Univ. Press, Cambridge, England, U.K., 2001, pp. 331–340.

[9]Moran, J., An Introduction to Theoretical and Computational Aerodynamics, Wiley, New York, 1984.

[10]Batchelor, G.K., An Introduction to Fluid Dynamics, Cambridge University Press, Cambridge, U.K., 1973.

[11]Goldstein, H., Classical Mechanics, 3rd edition, pp.3-4, 2003.

[12]Pachter, M., D'Azzo, J. J., and Proud, A. W., "Tight Formation Flight Control," *Journal of Guidance, Control, and Dynamics*, Vol. 24, No. 2, 2001, pp. 246–254. doi:10.2514/2.4735

[13]Anderson, J.D. Jr., Introduction to Flight, 3rd ed. McGraw Hill Publishing Co., New York, N.Y., 1989.

[14]Streeter, V.L., and Wylie, E.B., Fluid Mechanics, McGraw Hill Publishing Co., Seventh ed. New York, N.Y., 1979.

[15]Sarkka, S., Bayesian Filtering and Smoothing, Cambridge University Press, Cambridge, U.K., 2013.

[16]Hemati, M. S., Eldredge, J. D., and Speyer, J. L., "Wake Sensing for Aircraft Formation Flight," *AIAA Guidance, Navigation, and Control Conference*, AIAA Paper 2012-4768, Aug. 2012, doi:10.2514/6.2012-4768.

[17] Yeo, D., Sydney, N., Paley, D.A., and Sofge, D., "Onboard flow sensing for downwash detection and avoidance with a small quadrotor helicopter." In *Proc. AIAA Guidance Navigation and Control Conference*, number AIAA 2015-1769, pages 1–11, Orlando, Florida, January 2015.